Supplement of Biogeosciences, 14, 5533–5549, 2017
https://doi.org/10.5194/bg-14-5533-2017-supplement

Biogeosciences Open Access EGU

Supplement of

Exploring the contributions of vegetation and dune size to early dune development using unmanned aerial vehicle (UAV) imaging

Marinka E. B. van Puijenbroek et al.

Correspondence to: Marinka E. B. van Puijenbroek (marinka.vanpuijenbroek@gmail.com)

SUPPORTING INFORMATION

Dunes from above: exploring the contributions of vegetation and dune size to early dune building

Marinka E.B. van Puijenbroek, Corjan Nolet, Alma V. de Groot, Juha Suomalainen, Michel J.P.M. Riksen, Frank Berendse and Juul Limpens

Supplement S1 Weather conditions

Fig. S1.1 The wind speed and direction for the years 2013 - 2016. The wind rose shows the percentage the wind came from a certain direction over the time-period 2013 - 2016. The colours show the wind speed in m s^{-1}.

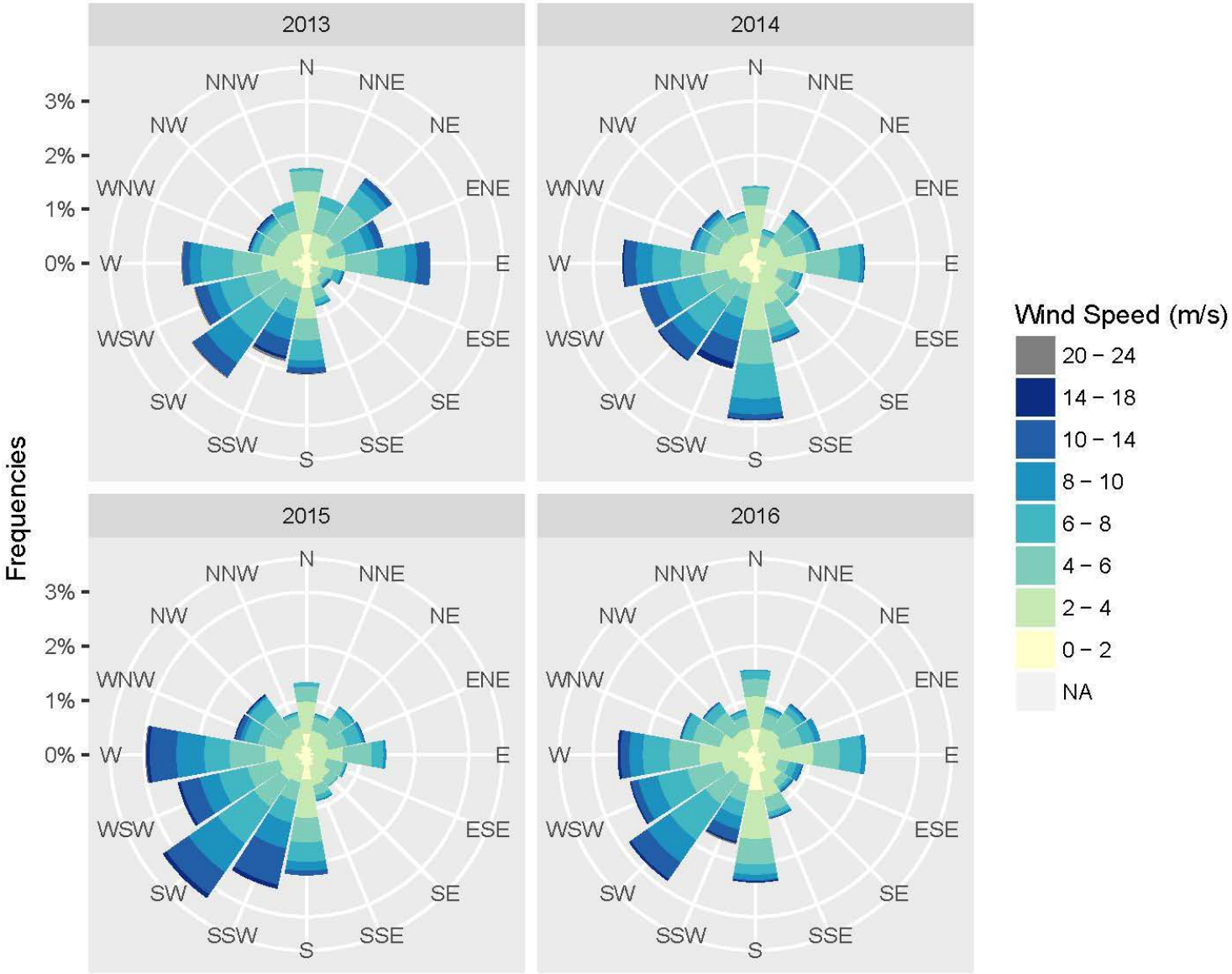

Table S1.1 Weather conditions in the years 2013 – 2016. For temperature the average is shown, and the precipitation was summed. For the precipitation in summer we summed the precipitation between the months April - August

Year	Temp. June & July (°C)	Temp. Januari & Februari (°C)	Total precipitation (mm)	Precipitation Summer (mm)
2013	15.67	2.25	553.2	163.1
2014	17.40	5.96	714.8	360.6
2015	15.98	4.47	804	283.8
2016	16.38	4.90	708.2	275.9

Table S1.2 Storm intensity in the years 2013 – 2016. The storm duration is calculated as the time the water level is above the water level recurrence of once a year.

Year	Storm duration (min)	Maximum water level (cm)
Winter 2013 - 2014	530	254
Winter 2014 - 2015	410	248
Winter 2015 - 2016	10	211

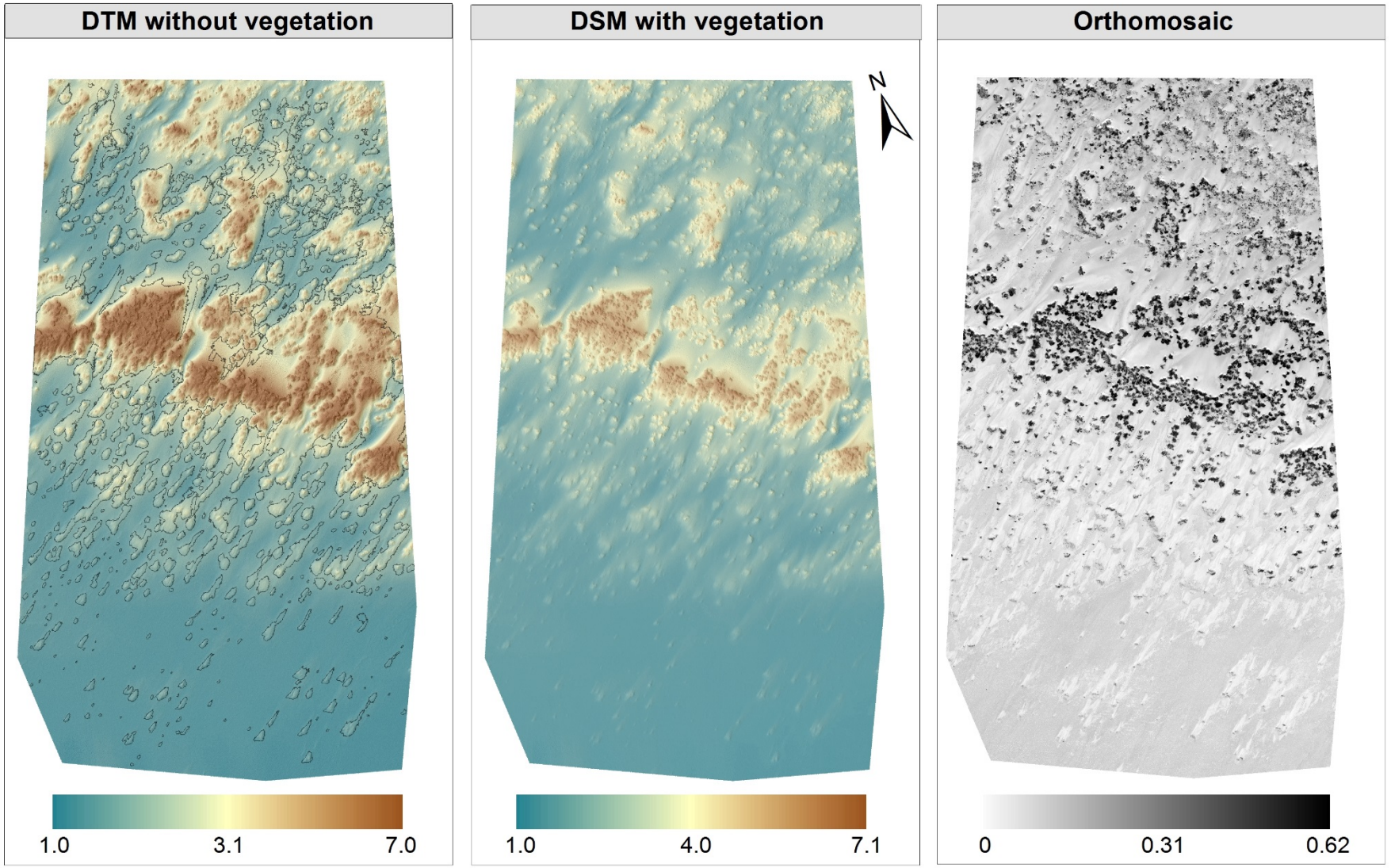

Figure S2.1 For the mapping campaign of August 2016 a digital terrain model with vegetation, a digital surface model without vegetation and an orthomosiac with NDVI values are shown. The legend bar for the DTM and DSM shows the elevation, and for the Orthomosaic the NDVI values.

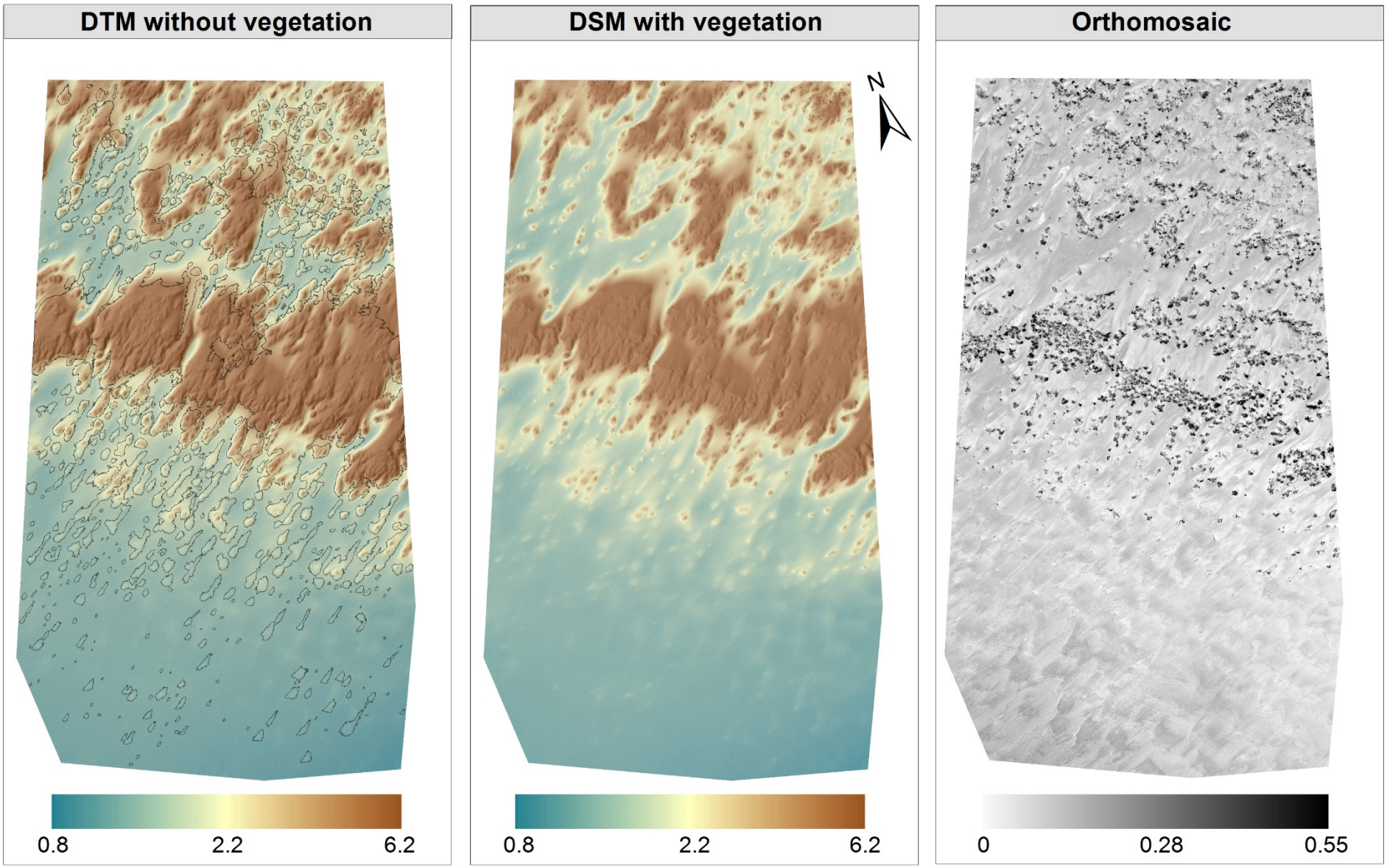

Figure S2.1 For the mapping campaign of April 2016 a digital terrain model with vegetation, a digital surface model without vegetation and an orthomosiac with NDVI values are shown. The legend bar for the DTM and DSM shows the elevation, and for the Orthomosaic the NDVI values.

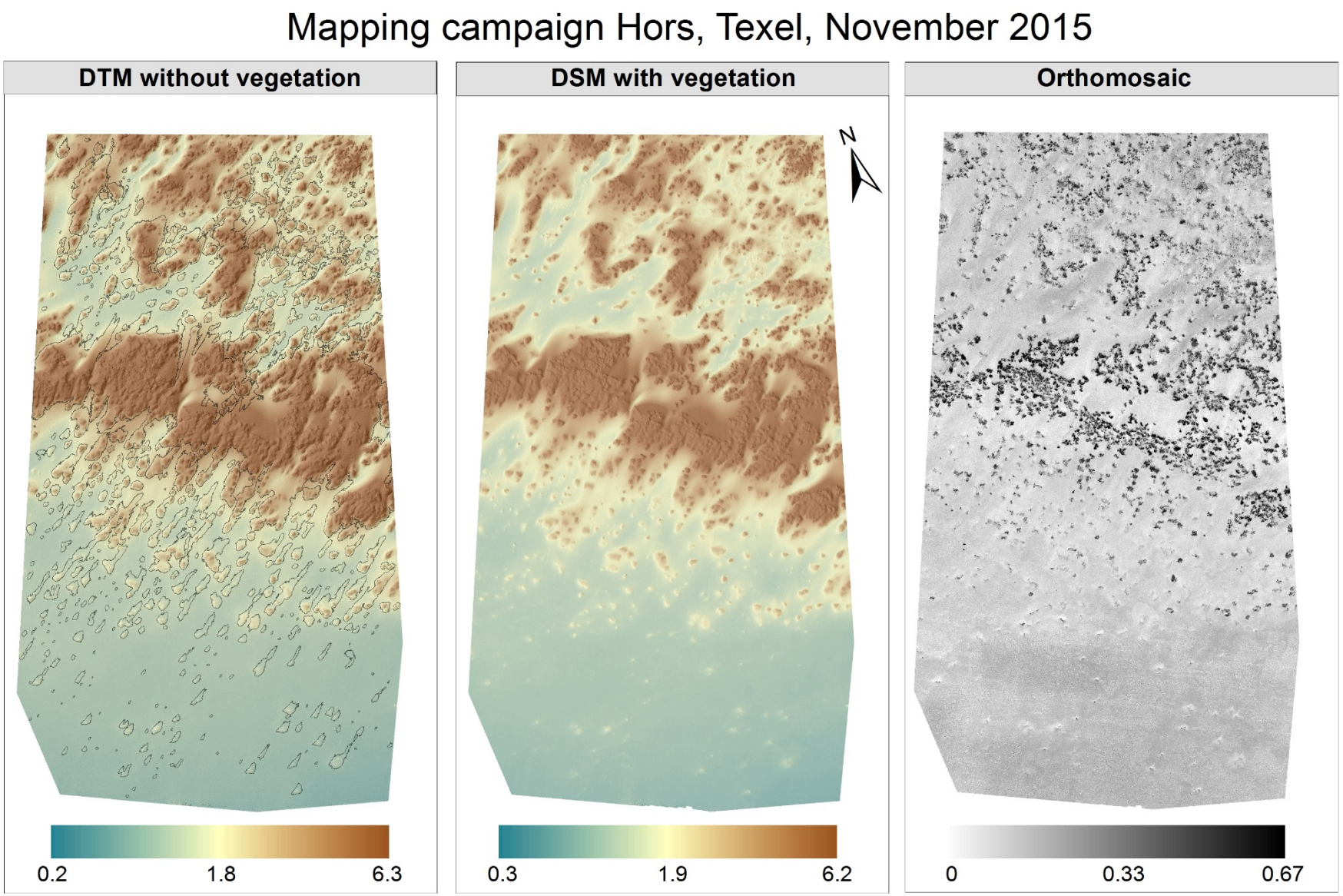

Figure S2.1 For the mapping campaign of November 2015 a digital terrain model with vegetation, a digital surface model without vegetation and an orthomosiac with NDVI values are shown. The legend bar for the DTM and DSM shows the elevation, and for the Orthomosaic the NDVI values.

Supplement S3 Dune morphology selected dunes

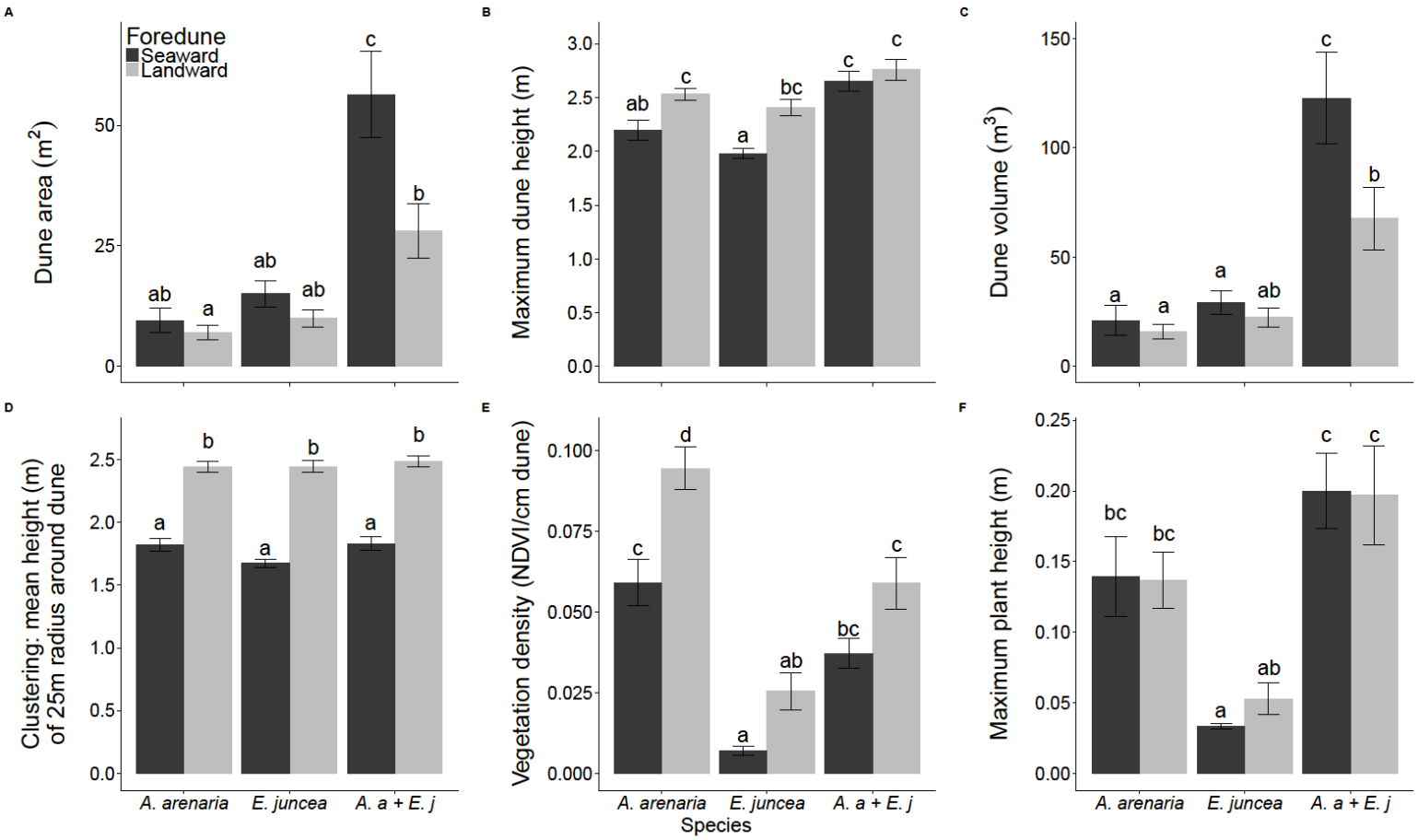

Fig. S3.1 Different dune characteristics for dunes with the blocks *A. arenaria*, *E. juncea* and a mix of both species separated for dune seaward and landward of the foredune: A) Dune area (m^2), B) Maximum dune height (m NAP), C) Dune volume (m^3), D) Clustering: mean height (m NAP) around a 25m radius around the dune, E) Vegetation density (NDVI/cm), F) Plant height (m), The letters denote the significant difference between the bars.

Supplement S4 Accuracy photogrammetric reconstruction

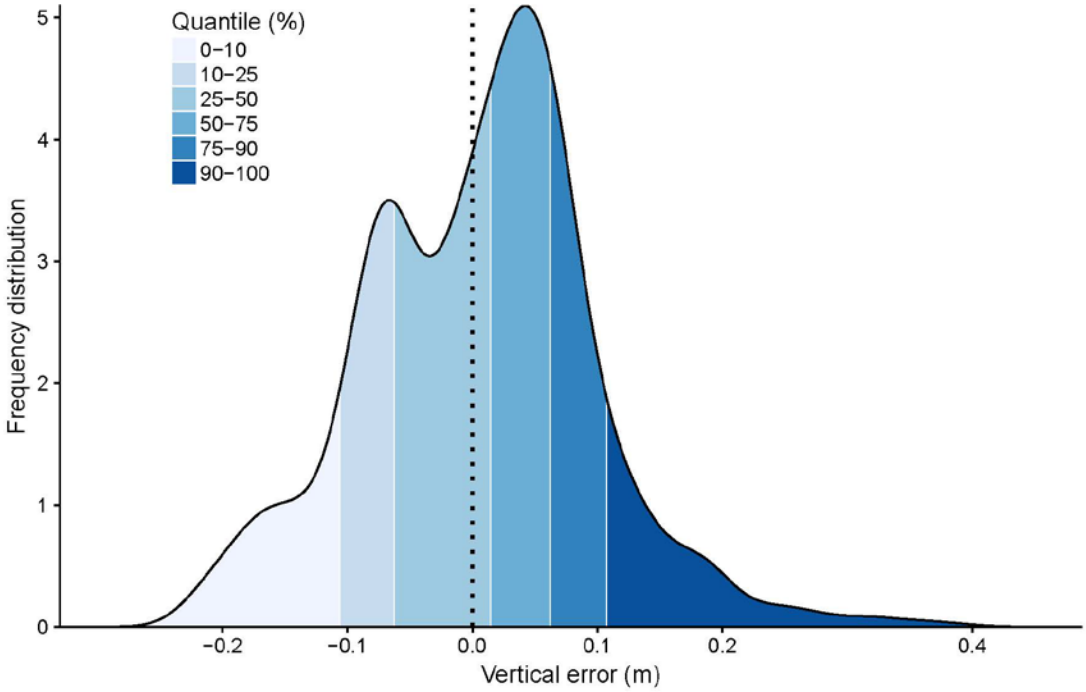

Figure S4.1 The frequency distribution of the vertical error (m) of the digital terrain model. The vertical error was calculated by subtracting the actual elevation measured with a RTK-DGPS Trimble R6 Model 3 (TSC3) from the elevation of the digital terrain model (without vegetation). The colours indicate the quantile distribution.

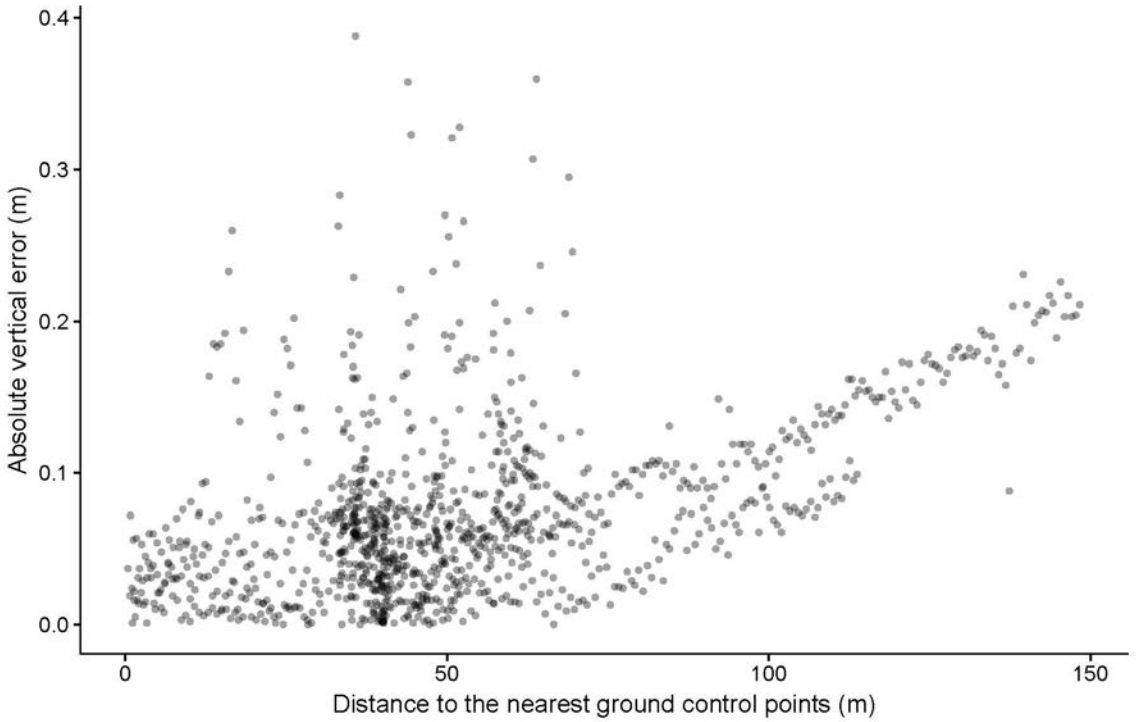

Figure S4.2 The relationship between the distance to the nearest ground control points (m) to the absolute vertical error (m).

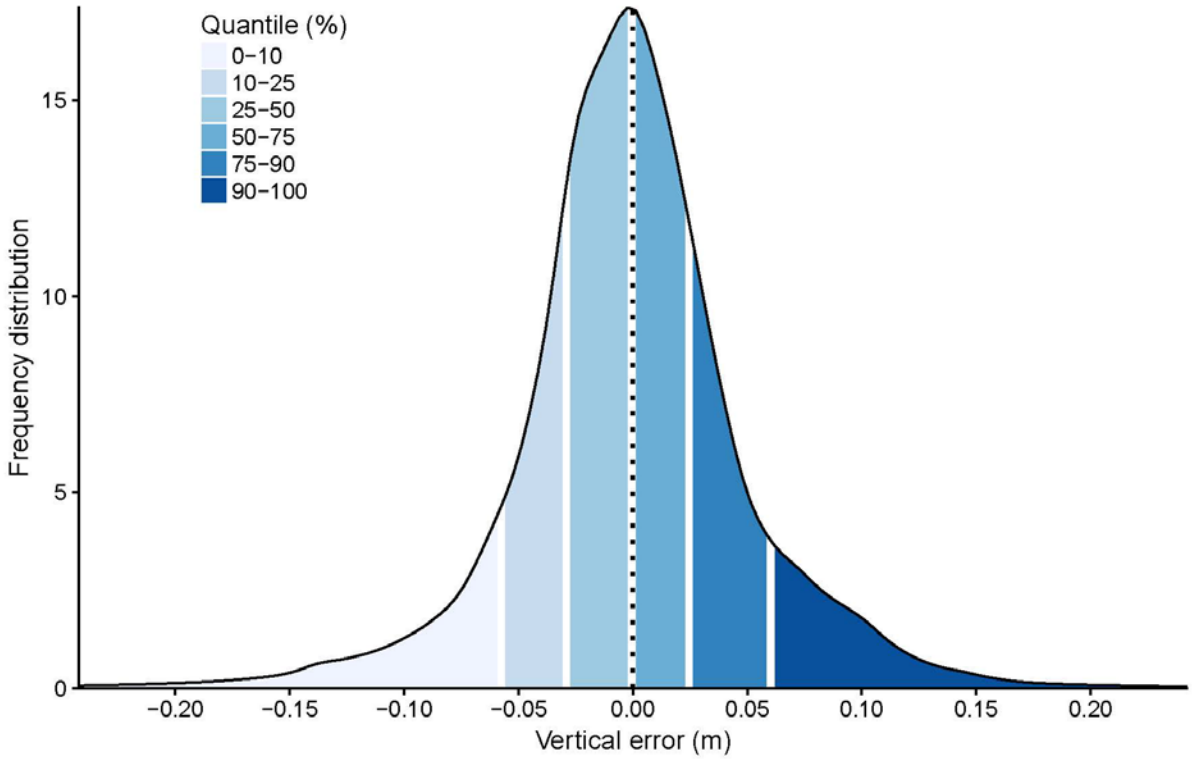

Figure S4.3 The frequency distribution of the vertical difference between repeated flights of the same flight path at the same day. The colours indicate the quantile distribution.

Table S4.1 The deviation of the nebka dune volume for different dune sizes for a vertical error of 10 cm and 20 cm.

Area	Mean elevation	Volume	Deviation (%) for 10 cm error	Deviation (%) for 20 cm error
0.51	2.83	1.45	3.57	7.10
2.54	2.05	5.22	4.89	9.75
5.01	2.16	10.84	4.62	9.24
10.18	2.48	25.26	4.03	8.06
20.25	1.70	34.42	5.88	11.77
50.73	2.28	115.66	4.39	8.77
156.30	2.21	344.85	4.53	9.07
16967.23	3.80	64444.20	2.63	5.27

Table S4.2 Overview of characteristics of optimized dense point clouds obtained with the Structure-from-Motion algorithm applied in the Agisoft Photoscan software for the three different mapping campaigns.

Mapping campaign	**August 2016**	**April 2016**	**November 2016**
Number of alinged camera's	844	827	872
Number of points dense point cloud	71,354,624	77,189,711	75,327,967
Effective overlap (%)	6.1	4.9	5.1
Estimated mean point density (n m^{-2})	573	648	612
Mean reprojection error (pixels)	0.52	1.13	1.17
Flying altitude (m)	79.6	72.1	75